

Shape oscillation and stability of an encapsulated microbubble translating in an acoustic wave

Yunqiao Liu, Michael L. Calvisi, and Qianxi Wang^{3,a)}

(Received 26 May 2018; revised 14 September 2018; accepted 17 September 2018; published online 15 October 2018)

Encapsulated microbubbles (EMBs) are associated with a wide variety of important medical applications, including sonography, drug delivery, and sonoporation. The nonspherical oscillations, or shape modes, of EMBs strongly affect their stability and acoustic signature, and thus are an important factor to consider in the design and utilization of EMBs. Under acoustic forcing, EMBs often translate with significant velocity, which can excite shape modes, yet few studies have addressed the effect of translation on the shape stability of EMBs. In this work, the shape stability of an EMB subject to translation is investigated through development of an axisymmetric model for the case of small deformations. The potential flow in the bulk volume of the external flow is modeled using an asymptotic analysis. Viscous effects within the thin boundary layer at the interface are included, owing to the no-slip boundary condition, using Prosperetti's theory [Q. Appl. Math. 34, 339 (1977)]. In-plane stress and bending moment due to the encapsulation are incorporated into the model through the dynamic boundary condition at the interface. The evolution equations for radial oscillation, translation, and shape oscillation of an EMB are derived, which can be reduced to model an uncoated gas bubble by neglecting the encapsulation properties. These equations are solved numerically to analyze the shape mode stability of an EMB and a gas bubble subject to an acoustic, traveling plane wave. The findings demonstrate the counterintuitive result that translation has a more destabilizing effect on an EMB than on a gas bubble. The no-slip condition at the encapsulating membrane is the main factor responsible for mediating this interfacial instability due to translation. © 2018 Acoustical Society of America. https://doi.org/10.1121/1.5058403

[CCC] Pages: 2189–2200

I. INTRODUCTION

Encapsulated microbubbles (EMBs) are finding widespread use in biomedicine and are attracting increasing attention from the scientific community. Ultrasound contrast agents (UCAs) were developed for enhancing contrast in ultrasound imaging and represent one of the most successful applications of EMBs. In addition to diagnostic purposes, the application of EMBs is expanding to include therapies such as drug delivery, gene therapy, and tissue ablation, among others. 1-3 For both diagnostic and therapeutic applications, the EMB interacts with an applied ultrasound field, which drives the volume (radial) mode and can excite nonspherical shape oscillations as well. Shape oscillations strongly influence the stability of the membrane and, therefore, impact the overall efficacy of EMBs. For example, in sonography, UCA stability is important to maintain in order to maximize residence time. Furthermore, stable shape oscillations help generate subharmonic, harmonic, and ultraharmonic frequency components that enhance the acoustic signature of UCAs and improve image contrast.^{4,5} In

In addition to volume and shape oscillation, the ultrasound field can incite translation of the EMB directly via the primary Bjerknes force and indirectly due to the secondary Bjerknes force, e.g., due to the presence of nearby tissue surfaces and/or bubbles. 6,7 Translation of an EMB is coupled to both the radial and shape dynamics, as is well documented for uncoated gas bubbles. 8-18 A number of theoretical, numerical, and experimental studies have investigated the radial and shape dynamics of EMBs, 19-27 but the role of translation has received less attention. However, microbubbles subject to ultrasonic forcing can translate at relatively large velocities, which can be an important mechanism for the effective use of EMBs in biomedicine, e.g., for sonoporation. 28,29 Thus, a complete understanding of the dynamics of EMBs under acoustic forcing must include the effect of translation, which motivates the present work.

The coupling of shape oscillation and translation of uncoated gas bubbles in a standing wave, known as the "dancing bubble problem," was observed experimentally by Strasberg and Benjamin³⁰ and Crum and Eller.³¹ A similar

¹Key Laboratory of Hydrodynamics (Ministry of Education), School of Naval Architecture, Ocean and Civil Engineering, Shanghai Jiao Tong University, Shanghai, 200240, China

²Department of Mechanical and Aerospace Engineering, University of Colorado, Colorado Springs, Colorado 80918, USA

³School of Mathematics, University of Birmingham, Birmingham, B15 2TT, United Kingdom

therapeutic applications, unstable shape oscillation can promote rupturing of the EMB coating, which can affect the localized release of therapeutic agents within the circulatory system.

a)Electronic mail: q.x.wang@bham.ac.uk

phenomenon has been observed in gas bubbles for the case of traveling acoustic waves by Dayton et al. Theoretical studies of the shape oscillation of gas bubbles have been conducted by several researchers and have provided insight into the coupling among the radial oscillation, shape modes, and translation. 10,12,14–18,32–37 The translation of EMBs subject to an ultrasound wave has also been studied without considering their shape deformations.³⁸

In this theoretical study, the dynamics and shape stability of both uncoated and EMBs subject to an acoustic, traveling plane wave are studied through consideration of the coupling of radial oscillation, translation, and shape modes. It is assumed that the external flow is potential in the bulk volume except for a thin viscous boundary layer near the EMB-liquid interface. The potential flow is modeled using an asymptotic analysis. Viscous effects within the thin boundary layer at the interface are approximated using Prosperetti's theory.³⁹ To consider the influence of the shell on the EMB dynamics, the in-plane stress and bending moment of the encapsulation are incorporated into the dynamic boundary condition at the interface. The amplitudes of the shape modes are assumed small with respect to the radius of the volume mode, which permits the use of perturbation methods to derive evolution equations governing the radial (volume) oscillation, translation, and shape oscillations of an EMB. This model is readily reduced to an uncoated gas bubble by neglecting the encapsulation properties (e.g., shell stiffness and viscosity). The governing equations are solved numerically in order to analyze the shape dynamics and stability of a gas bubble and an EMB subject to an acoustic, traveling plane wave over a range of frequencies and amplitudes with clinical relevance. While translation is shown to reduce stability in both cases, it has a much stronger destabilizing effect on EMBs compared to uncoated gas bubbles. We find that the no-slip condition at the EMB interface is the main factor responsible for this reduction in stability.

In Sec. II, we develop the theoretical model for the dynamics of an EMB that includes radial and shape mode oscillations, along with translation. The results of numerical analyses for both uncoated gas bubbles and EMBs are presented in Sec. III, and physical insights based on these results are discussed. Last, a summary of the main findings and conclusions of this work is given in Sec. IV.

II. PROBLEM FORMULATION

In this section, we derive the mathematical formulation for the dynamics of an encapsulated bubble translating subject to a traveling acoustic wave. We consider the axisymmetric deformation of the bubble and establish a local coordinate system (x,y,z,t) with the origin at the bubble geometric center upon a ground fixed coordinate system (X,Y,Z,T), as illustrated in Fig. 1. The symmetry axis Oz is parallel to the translational direction of the bubble centroid (see Fig. 1). The transformation between the local coordinates (x,y,z,t) and the ground fixed coordinates (X,Y,Z,T) is

$$t = T, \quad x = X, \quad y = Y, \quad z = Z - Z_{bc}(t),$$

$$\frac{\partial}{\partial T} = \frac{\partial}{\partial t} - \dot{Z}_{bc}(t) \frac{\partial}{\partial z}, \quad \left(\frac{\partial}{\partial x}, \frac{\partial}{\partial y}, \frac{\partial}{\partial z}\right) = \left(\frac{\partial}{\partial X}, \frac{\partial}{\partial Y}, \frac{\partial}{\partial Z}\right),$$
(1)

where Z_{bc} is the z-coordinate of the bubble center in the ground fixed system.

The encapsulated bubble is subject to an acoustic wave. The traveling plane wave with frequency ω_d applies an acoustic pressure, $p_{\rm ac}$, in the ground fixed system,

$$p_{\rm ac} = \varepsilon p_0 \sin\left(\frac{\omega_d}{c_l} Z - \omega_d t\right),\tag{2}$$

where p_0 is the ambient pressure, ε is the dimensionless amplitude of the wave, and c_l is the speed of sound in the liquid. The flow velocity, v_{ac} , induced by the acoustic pressure obeys the linear Euler equation,

$$\rho \frac{\partial v_{\rm ac}}{\partial t} \mathbf{e}_z = -\nabla p_{\rm ac},\tag{3}$$

where ρ is the liquid density. Substituting Eq. (2) into Eq. (3) and integrating in time yields the induced flow velocity

$$v_{\rm ac} = \frac{\varepsilon p_0}{\rho c_l} \sin\left(\frac{\omega_d}{c_l} Z - \omega_d t\right). \tag{4}$$

Since the bubble size is much smaller than the wavelength of the acoustic wave $(R \ll c_l/\omega_d)$, where R is bubble radius), the velocity due to the acoustic wave at the bubble surface, v_a , is approximately

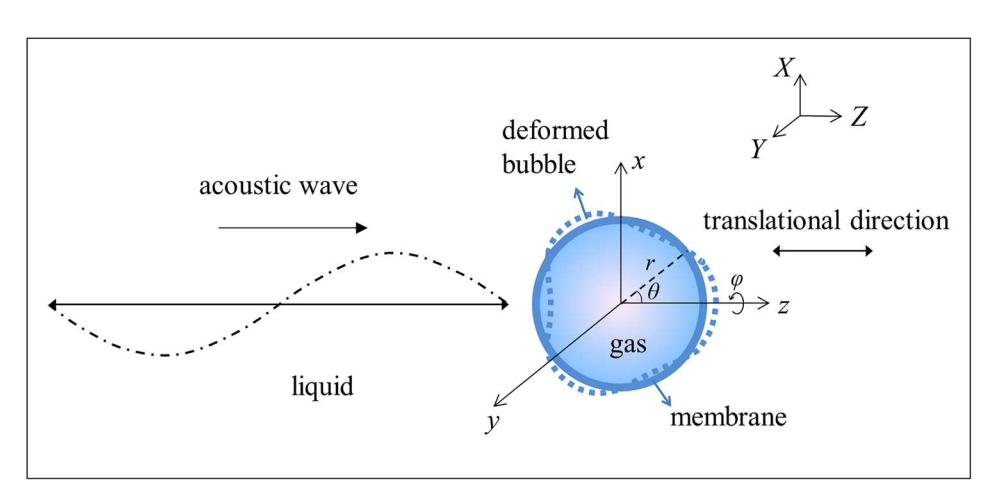


FIG. 1. (Color online) The configuration and coordinate system for a translating encapsulated bubble subject to a traveling acoustic wave.

$$v_a = \frac{\varepsilon p_0}{\rho c_l} \sin\left(\frac{\omega_d}{c_l} Z_{bc} - \omega_d t\right). \tag{5}$$

The velocity, \mathbf{u} , and the pressure, p, of the liquid flow field are governed by the incompressible Navier-Stokes equations

$$\nabla \cdot \mathbf{u} = 0, \tag{6}$$

$$\rho \frac{\partial \mathbf{u}}{\partial t} + \rho (\mathbf{u} - \dot{Z}_{bc} \mathbf{e}_z) \cdot \nabla \mathbf{u} = -\nabla p + \mu_l \nabla \cdot (\nabla \mathbf{u} + \nabla \mathbf{u}^T),$$
(7)

where μ_l is the liquid viscosity. We neglect the flow field within the bubble due to the negligible density and viscosity of the interior gas as compared to the external liquid.

We assume that the bubble is approximately spherical, and translates while undergoing appreciable radial oscillations and small amplitude shape oscillations. The shape perturbation to a spherical bubble can be expanded in terms of spherical harmonics. With the restriction to axisymmetric deformation, the spherical harmonics reduce to the Legendre polynomials, as the azimuthal mode is constant. The position of a material point on the membrane is expressed in terms of the radial, r, and tangential, Θ , directions as follows:

$$r(\theta, t) = R(t) + \sum_{k=2}^{\infty} a_k(t) P_k(\cos \theta),$$
 (8)

$$\Theta(\theta, t) = \theta + \frac{1}{R(t)} \sum_{k=1}^{\infty} b_k(t) P_k^1(\cos \theta), \tag{9}$$

where R is the radius of the unperturbed spherical mode, and a_k and b_k are the shape distortion amplitudes in the radial and tangential directions, respectively. We assume $a_k,b_k \ll R$. The series of the Legendre polynomials, $P_k(\cos\theta)$, represent the perturbations of the membrane in the radial direction with shape mode amplitudes a_k . The summation in Eq. (8) is from k=2, since k=1 is associated with the translation of the bubble, which is treated separately through the translational velocity. The series of the associated Legendre polynomials, $P_k^1(\cos\theta) = dP_k(\cos\theta)/d\theta$, represent shape perturbations in the tangential direction with amplitudes b_k , in which b_1 denotes the displacements of material points along the bubble interface with its shape keeping spherical.

We assume the viscous effects are confined to a thin, liquid boundary layer adjacent to the membrane, and solve for the velocity and pressure by decomposing them into the potential (irrotational) part and the viscous (rotational) correction

$$\mathbf{u} = \mathbf{u}_p + \mathbf{u}_v,\tag{10}$$

$$p = p_p + p_v, \tag{11}$$

where the subscripts p and v refer to the potential and viscous parts, respectively.

The velocity potential satisfies Laplace's equation, owing to the incompressibility condition (6). The flow field induced by the acoustic pressure is superimposed on that induced by the bubble dynamics, thus, the velocity potential can be expressed as

$$\varphi = v_a r P_1(\cos \theta) + \sum_{k=0}^{\infty} \frac{q_k}{r^{k+1}} P_k(\cos \theta), \tag{12}$$

where q_k are the coefficients to be determined by the kinematic boundary condition,

$$\frac{\partial S}{\partial t} + \left(\nabla \varphi - \dot{Z}_{bc} \mathbf{e}_z\right) \cdot \nabla S = 0, \tag{13}$$

where $\nabla \varphi$ is the liquid velocity due to the potential part of the flow, and S is the surface function

$$S(r, \theta, t) \equiv r - R(t) - \sum_{k=2}^{\infty} a_k(t) P_k(\cos \theta) = 0.$$
 (14)

Making use of the orthogonality of the Legendre polynomials, we obtain the coefficients q_k for each mode as follows (see the Appendix for details):

$$q_0 = -\dot{R}R^2,\tag{15}$$

$$q_1 = -\frac{R^3}{2}v_r + \frac{3}{10}R^2v_r a_2,\tag{16}$$

$$q_{k} = -\frac{R^{k+2}}{k+1} \left(\dot{a}_{k} + \frac{2\dot{R}}{R} a_{k} \right) + \frac{3k}{2} R^{k+1} v_{r} \left(\frac{a_{k+1}}{2k+3} - \frac{a_{k-1}}{2k-1} \right), \tag{17}$$

where $v_r = \dot{Z}_{bc} - v_a$ is the relative velocity. The velocity of the potential part is obtained subsequently from $\mathbf{u}_p = \nabla \varphi$, which leads to

$$\mathbf{u}_{p} = \frac{\partial \varphi}{\partial r} \mathbf{e}_{r} + \frac{1}{r} \frac{\partial \varphi}{\partial \theta} \mathbf{e}_{\theta}. \tag{18}$$

The pressure of the potential flow is obtained by the Bernoulli equation

$$p_p = p_0 + p_{\rm ac} - \rho \left[\frac{\partial \varphi}{\partial t} + \frac{1}{2} |\nabla \varphi|^2 - \dot{Z}_{\rm bc} \mathbf{e}_z \cdot \nabla \varphi \right]. \tag{19}$$

Equation (19) is obtained based on the weakly compressible theory. ⁴⁰ In the theory, the flow in the outer region, far away from the bubble with the scale of the wavelength of the acoustic wave, is shown to satisfy the linear wave equation to second order in terms of the Mach number. The flow in the inner region is shown to satisfy Laplace's equation to second order. The far-field conditions of the inner region are $(\partial \phi_{\rm ac}/\partial t)|_{r\to\infty} = -(p_{\rm ac}/\rho)$ and $p_{\infty} = p_0 + \varepsilon p_0 \sin{(\omega_d t)}$, which are used to derive Eq. (19).

Due to the no-slip condition at the interface of an encapsulated bubble, vorticity is generated due to the tangential motion of the interface and diffuses into the flow field, which, in turn, modifies the shear stress of the surrounding liquid. Therefore, viscous effects in the liquid cannot be neglected. In addition to the potential solution, we consider weak viscous effects and solve the viscous correction by following Prosperetti's theory. The viscous correction is obtained by decomposing vorticity into poloidal, $Q_k(r,t)$, and toroidal, $T_k(r,t)$, fields

$$\nabla \times \mathbf{u}_{v} = \sum_{k=1}^{\infty} [\nabla \times \nabla \times (Q_{k}(r, t) P_{k}(\cos \theta) \mathbf{e}_{r}) + \nabla \times T_{k}(r, t) P_{k}(\cos \theta) \mathbf{e}_{r}].$$
(20)

Only the toroidal field $T_k(r,t)$ is relevant since we consider an axisymmetric model, which is governed by the following equation:³⁹

$$\rho \frac{\partial T_k}{\partial t} + \rho \frac{\partial}{\partial r} \left[\dot{R} (R/r)^2 T_k \right] - \mu_l \frac{\partial^2 T_k}{\partial r^2} + \mu_l k(k+1) \frac{T_k}{r^2} = 0.$$
(21)

The viscous part of the velocity can be expressed in terms of the toroidal field as follows:

$$\mathbf{u}_{\nu} = \left(\sum_{k=1}^{\infty} T_k P_k - \frac{\partial \Phi}{\partial r}\right) \mathbf{e}_r - \frac{1}{r} \frac{\partial \Phi}{\partial \theta} \mathbf{e}_{\theta}, \tag{22}$$

where

$$\Phi = \sum_{k=1}^{\infty} \frac{k+1}{2k+1} P_k \left[\left(-\int_R^{\infty} s^{-k} T_k(s,t) ds + \int_R^r s^{-k} T_k(s,t) ds \right) r^k + \frac{k}{2k+1} \right] \times \left(-R^{2k+1} \int_R^{\infty} s^{-k} T_k(s,t) ds + \int_R^r s^{k+1} T_k(s,t) ds \right) r^{-(k+1)} ,$$
(23)

where *s* is the integration variable. The viscous correction to the pressure is evaluated at the bubble interface as

$$p_{\nu}|_{r=R} = \sum_{k=1}^{\infty} k \left\{ \mu_{l} T_{k}(R, t) / R + \rho(\dot{R} / R) \right.$$

$$\times \int_{R}^{\infty} \left[(R/s)^{3} - 1 \right] (R/s)^{k} T_{k}(s, t) ds \right\} P_{k}(\cos \theta).$$
(24)

The partial differential equation (21) will be solved numerically based on the boundary conditions given below.

The flow velocity \mathbf{u} satisfies the stress balance at the bubble interface.

$$\mathbf{n} \cdot \left[-p\mathbf{I} + 2\mu_l (\nabla \mathbf{u} + \nabla \mathbf{u}^T) \right] + p_g \mathbf{n} - (\gamma \nabla \cdot \mathbf{n}) \mathbf{n} = \mathbf{F},$$
(25)

where **I** is the unit tensor, **n** is the outward unit normal vector of the interface S, γ is the surface tension, and **F** is the membrane stress. The stress balance [Eq. (25)] includes the pressures due to the gas and the liquid, the viscous stress on the liquid side, and the membrane stress (for EMBs only) or surface tension (for gas bubble only). Note that when a bubble is coated by a membrane, the surface tension is effectively negligible, replaced by the membrane stress. Therefore, we set $\gamma = 0$ for EMB cases and $\mathbf{F} = 0$ for gas bubble cases. The liquid pressure p is given by Eq. (11), which includes the

potential part [Eq. (19)] and viscous correction [Eq. (24)]. Due to the encapsulation, mass transport to and from the bubble is neglected, along with the presence of vapor. Therefore, the internal bubble pressure, p_g , is due to only a noncondensible gas, which is assumed to be spatially uniform and undergoes an adiabatic process according to the polytropic relation,

$$p_g = p_{g0} \left(\frac{V_0}{V}\right)^{\Gamma},\tag{26}$$

where V is the bubble volume at the current time, the subscript 0 indicates the initial value, and Γ is the ratio of specific heats of the bubble gas. The membrane stress, \mathbf{F} , is given by the surface divergence of the elastic stress tensor⁴¹

$$\mathbf{F} = -(\mathbf{P} \cdot \nabla) \cdot (\mathbf{\tau} + \mathbf{q}\mathbf{n}),\tag{27}$$

where $\mathbf{P} = \mathbf{I} - \mathbf{n} \mathbf{n}$ is the tangential projection operator, $\boldsymbol{\tau}$ is the in-plane stress, and \mathbf{q} is the transverse shear stress, which is expressed in terms of bending moment \mathbf{m} as, $\mathbf{q} = [(\mathbf{P} \cdot \nabla) \cdot \mathbf{m}] \cdot \mathbf{P}$. We model the membrane as a viscoelastic material, employing the neo-Hookean law⁴² for the inplane stress, a linear law for the membrane viscosity, and the Love law⁴³ for the bending moments. The expression for the membrane stress is based on Liu *et al.*²⁴ The surface tension, γ , is included here so that our model can be applied to gas bubbles by setting the membrane stress \mathbf{F} in Eq. (25) to zero. For encapsulated bubbles, the surface tension is set to zero.

Substituting the derived velocity and pressure into the dynamic boundary condition [Eq. (25)] and using the orthogonality of the Legendre polynomials, we obtain the dynamic equations for the bubble interface, of which the zeroth-order equation (k = 0) governs the radial oscillation,

$$R\ddot{R} + \frac{3}{2}\dot{R}^{2} + \frac{1}{\rho}\left[p_{0} + p_{ac} - p_{g0}\left(\frac{R_{0}}{R}\right)^{3\Gamma} + \frac{2\gamma}{R} + 4\mu_{l}\frac{\dot{R}}{R}\right] - \frac{v_{r}^{2}}{4} + \frac{v_{a}^{2}}{2} + v_{a}v_{r} = -\frac{1}{\rho}\left[\frac{2G_{s}\left(R^{6} - R_{0}^{6}\right)}{R^{7}} + 4\mu_{s}\frac{\dot{R}}{R^{2}}\right],$$
(28)

where G_s is the elastic modulus and μ_s is the membrane viscosity. Equation (28) is an extended Rayleigh-Plesset equation for a translating EMB. The term in square brackets on the right-hand side is associated with the membrane elasticity and viscosity, and the last three terms on the left-hand side are associated with the bubble translation and the flow velocity due to the acoustic wave. Equation (28) reduces to the Rayleigh-Plesset equation if the elasticity and viscosity of the membrane and the translation velocity are omitted.

The first-order mode (k=1) of the dynamic boundary condition governs the translational motion, written in the form of the inertia of the added mass and forces

$$\frac{d}{dt}\left(\frac{1}{2}\rho V v_r\right) = F_B + F_h + F_\mu + F_m,\tag{29}$$

where

$$\begin{split} F_{B} &= \rho V \dot{v}_{a}, \\ F_{h} &= \rho V \left[\frac{9 \dot{a}_{2}}{10 R} v_{r} + a_{2} \left(\frac{6 \dot{R}}{5 R^{2}} v_{r} + \frac{7}{10 R} \dot{v}_{r} + \frac{2}{5 R} \dot{v}_{a} \right) \right], \\ F_{\mu} &= -12 \pi \mu_{l} R v_{r} + 8 \pi \mu_{l} R \int_{R}^{\infty} \frac{T_{1}(s,t)}{s} ds \\ &- \rho V \frac{\dot{R}}{R^{2}} \int_{R}^{\infty} \left[\left(\frac{R}{s} \right)^{3} - 1 \right] \left(\frac{R}{s} \right) T_{1}(s,t) ds, \\ F_{m} &= V \left[18 G_{s} \frac{R_{0}^{6}}{R^{9}} b_{1} + 3(1+v) G_{b} \frac{b_{1}}{R^{5}} - \frac{6 \mu_{s}}{R^{4}} \left(\dot{R} b_{1} - R \dot{b}_{1} \right) \right], \end{split}$$

$$(30)$$

where $V=(4/3)\pi R^3$, G_b is the bending modulus, and v is the Poisson ratio. The force F_B is related to the gradient of pressure, which provides the primary Bjerknes force. F_h is the effect of the second-order shape mode on translation. F_μ is the viscous effect, including the quasisteady drag and history force related to the unsteady diffusion of vorticity. $^{44}F_m$ is the membrane stress.

The dynamic equation for the higher-order modes $(k \ge 2)$ of shape oscillation is

$$M\ddot{a}_k + D\dot{a}_k + Wa_k + G_{k+1} + G_{k-1} = T + F_{mk},$$
 (31)

where

$$\begin{split} &M = \frac{R}{k+1}, \\ &D = \frac{3\dot{R}}{k+1} + \frac{2(k+2)\mu_l}{\rho R}, \\ &W = \left[-\frac{k-1}{k+1} \ddot{R} + \frac{(k+2)(k-1)\gamma}{\rho R^2} + \frac{4(k-1)\mu_l \dot{R}}{\rho R^2} - \frac{9(2k^4+3k^3+k^2+k-1)}{2(2k+1)(2k+3)} \frac{v_r^2}{R} \right], \\ &G_{k+1} = -\dot{a}_{k+1} v_r \frac{3(2k+1)}{2(2k+3)} - a_{k+1} \left[\frac{3(k+1)v_r \dot{R}}{(2k+3)R} + \frac{5k+2}{2(2k+3)} \dot{v}_r + \frac{k+1}{2k+3} \dot{v}_a + \frac{3(k+1)(k^2+2k+6)}{2k+3} \frac{\mu_l v_r}{\rho R^2} \right], \\ &G_{k-1} = \begin{cases} \frac{3}{4} v_r^2, & \text{for } k = 2 \\ \frac{3}{2} \dot{a}_{k-1} v_r + a_{k-1} \left[\frac{k}{2(2k-1)} (\dot{v}_r - 2\dot{v}_a) - \frac{3(1-k)}{2k-1} v_r \left(\frac{\dot{R}}{R} + k(k+4) \frac{\mu_l}{\rho R^2} \right) \right], & \text{for } k \geq 3 \end{cases} \\ &T = -k \frac{\mu_l}{\rho} \frac{T_k(R,t)}{R} + 2k(k+1) \frac{\mu_l}{\rho} R^{k-2} \int_R^\infty s^{-k} T_k(s,t) ds - k \frac{\dot{R}}{R} \int_R^\infty \left[\left(\frac{R}{s} \right)^3 - 1 \right] \left(\frac{R}{s} \right)^k T_k(s,t) ds, \\ &F_{mk} = \frac{G_s}{\rho R^8} \left[2(R^6 - 7R_0^6) a_k + 6k(k+1) R_0^6 b_k \right] - \frac{G_b}{\rho R^4} \left[k(k+1)(k^2+k-1+v)(a_k-b_k) \right] \\ &- \frac{2\mu_s}{\rho R^3} \left[-4a_k \dot{R} + 2R\dot{a}_k + k(k+1) (\dot{R}b_k - R\dot{b}_k) \right]. \end{aligned} \tag{32}$$

Due to the nature of the Legendre polynomials, the effects of adjacent shape modes a_{k+1} and a_{k-1} are included in terms G_{k+1} and G_{k-1} , respectively. The terms T and F_{mk} contain terms related to the toroidal field and membrane, respectively. Equation (31) is the equation for shape oscillation of a translating EMB. It reduces to the equation for the shape oscillation of gas bubbles given by Prosperetti³⁹ if the stress of the membrane and translational velocity are omitted.

The dynamic boundary condition [Eq. (25)] applied in the tangential direction provides the balance between the shear stress and the membrane tangential stress

$$2\mu_{l} \left[\frac{3\nu_{r}}{2R} - \frac{9a_{2}\nu_{r}}{10R^{2}} - \frac{T_{1}(R,t)}{2R} - R^{-1} \int_{R}^{\infty} s^{-1}T_{1}(s,t)ds \right]$$

$$= 6G_{s} \frac{R_{0}^{6}}{R^{8}} b_{1} + (1+v) \frac{G_{b}}{R^{4}} b_{1} + \frac{2\mu_{s}}{R^{3}} \left(R\dot{b}_{1} - \dot{R}\dot{b}_{1} \right), \tag{33}$$

for k = 1, and,

$$2\mu_{l} \left[\frac{k+2\dot{a}_{k}}{k+1} \frac{\dot{a}_{k}}{R} - \frac{k-1}{k+1} \frac{\dot{R}a_{k}}{R^{2}} + \frac{3k(k+2)}{2} \frac{v_{r}}{R^{2}} \left(\frac{a_{k-1}}{2k-1} \right) - \frac{a_{k+1}}{2k+3} \right) - R^{k-2} \int_{R}^{\infty} s^{-k} T_{k}(s,t) ds - \frac{T_{k}(R,t)}{2R} \right]$$

$$= \frac{G_{s}}{R^{8}} \left[(R^{6} - 7R_{0}^{6}) a_{k} + (3k(k+1)R_{0}^{6} + (k-1) + v)(a_{k} - k) \right]$$

$$\times (k+2)R^{6} b_{k} - \frac{G_{b}}{R^{4}} (k^{2} + k - 1 + v)(a_{k} - k) + \frac{2\mu_{s}}{R^{3}} \left[2a_{k}\dot{R} - R\dot{a}_{k} + (k^{2} + k - 1)(R\dot{b}_{k} - \dot{R}b_{k}) \right],$$

$$(34)$$

for $k \ge 2$. For a gas bubble, the free slip interface yields a shear-free condition, for which the right-hand sides of Eqs. (33) and (34) are zero.

The no-slip condition implies the continuity of tangential velocity, $u_{\theta} - \dot{Z}_{bc} \mathbf{e}_z \cdot \mathbf{e}_{\theta} = r(\partial \Theta/\partial t)$, leading to

$$-\frac{3}{2}v_r + \frac{3a_2}{10R}v_r + \int_R^\infty s^{-1}T_1(s,t)ds = \dot{b}_1 - \frac{\dot{R}}{R}b_1, \quad (35)$$

for k = 1, and,

$$-\frac{1}{k+1} \left(\dot{a}_k + \frac{2a_k \dot{R}}{R} \right) - \frac{3kv_r}{2R} \left(\frac{a_{k-1}}{2k-1} - \frac{a_{k+1}}{2k+3} \right) + R^{k-1} \int_{R}^{\infty} s^{-k} T_k(s,t) ds = \dot{b}_k - \frac{\dot{R}}{R} b_k,$$
 (36)

for $k \ge 2$.

Equations (28), (29), (31), and (35) or (36) are solved numerically for the unknown functions R(t), $v_r(t)$, $a_k(t)$, and $b_k(t)$ by using the fourth-order Runge-Kutta method. The toroidal field $T_{k}(r,t)$ is updated at every time step by solving Eq. (21) using the second-order finite difference method,²⁴ with the boundary condition $T_k(R,t)$ at the surface of an EMB obtained from (33) or (34) and the far field condition $T_k \rightarrow 0$ at infinity. The integrals in Eqs. (30) and (32)–(36) are calculated numerically by using the composite trapezoidal rule. For simulations of gas bubbles, b_k is set identically to zero and Eqs. (35) and (36) need not be solved.

III. NUMERICAL ANALYSES

In this section, we simulate the response of an EMB with $R_0 = 10 \,\mu\text{m}, \ G_s = 0.5 \,\text{N} \ \text{m}^{-1}, \ G_b = 1 \times 10^{-13} \,\text{N} \ \text{m}, \ \mu_s = 1$ \times 10⁻⁸ kg s⁻¹, and v = 0.5, which are within the intermediate range of property values for EMBs used in medical applications. 45 The external fluid is assumed to be water with density $\rho = 1000 \,\mathrm{kg \ m^{-3}}$ and viscosity $\mu_l = 1 \times 10^{-3} \,\mathrm{kg \ (m \ s)^{-1}}$. For comparison, the cases for a gas bubble have surface tension set to $\gamma = 0.0729 \,\mathrm{N m^{-1}}$. Under these parameters, the natural frequencies of radial mode, ω_0 , and shape modes, ω_k (k = 2-4), for the EMB and the gas bubble are calculated according to Liu and Wang⁴⁶ and Lamb⁴⁷ and shown in Table I.

The minimum acoustic pressure amplitude inducing shape instability is introduced as the instability threshold, ε_{thr} . Figure 2 displays the instability threshold versus frequency up to 1 MHz. Here we prescribe an initial disturbance to the shape modes $a_k(t=0)/R_0 = 10^{-4}$ for $k \ge 2$ and regard the interface shape unstable if $|a_k|/R_0 > 0.5$. Note that for the cases with translation, the stability diagram in Fig. 2 is obtained by solving the whole coupled system of equations, including the radial dynamic equation (28), the translation equation (29), and the shape oscillation equations (31) and (35) or (36). For the cases without translation, we fix the z-coordinate of the bubble center at the origin (i.e., set $Z_{bc} = 0$ and $\dot{Z}_{bc} = 0$), set the flow velocity, v_a , induced by the acoustic pressure to zero, and do not solve the equations related to the translational mode [Eqs. (29), (33), and (35)];

TABLE I. Natural frequencies of the radial mode, ω_0 , and shape modes, ω_k (k=2, 3, and 4), where $R_0 = 10 \,\mu\text{m}$, $\rho = 1000 \,\text{kg m}^{-3}$, and $\mu_l = 1 \times 10^{-3} \,\text{kg}$ (m s)⁻¹, and $G_s = 0.5 \,\text{N m}^{-1}$, $G_b = 1 \times 10^{-13} \,\text{N m}$, $\mu_s = 1 \times 10^{-8} \,\text{kg s}^{-1}$, and v = 0.5 for an EMB, and $\gamma = 0.0729 \,\mathrm{N m^{-1}}$ for a gas bubble.

	$\omega_0/2\pi~(\mathrm{MHz})$	$\omega_2/2\pi~(\mathrm{MHz})$	$\omega_3/2\pi$ (MHz)	$\omega_4/2\pi~(\mathrm{MHz})$
EMB	0.51	0.25	0.32	0.38
Gas bubble	0.34	0.15	0.27	0.41

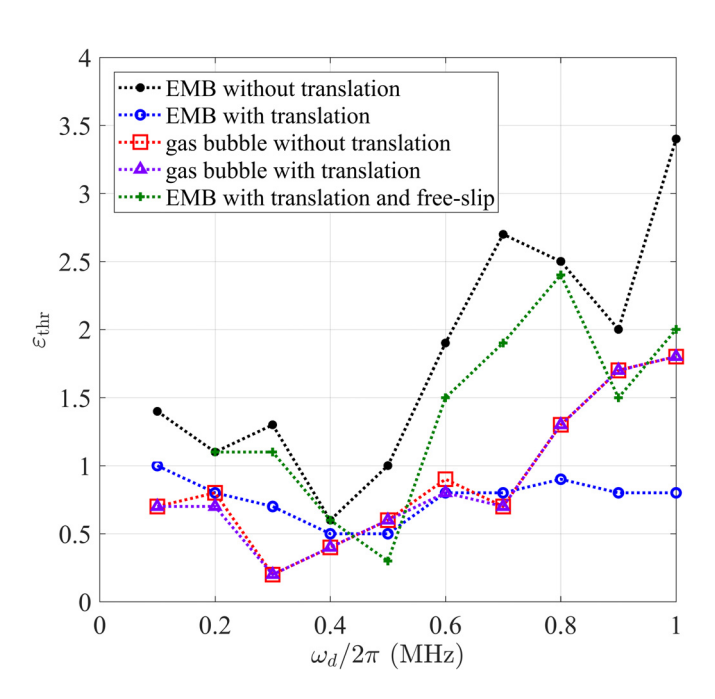


FIG. 2. (Color online) Threshold of acoustic pressure amplitude, ε_{thr} , for inducing shape instability versus driving frequency, ω_d . The remaining parameters are the same as in Table I.

thus, the relative velocity, v_r , remains zero. This process is equivalent to driving a bubble with a standing acoustic wave (assuming the wavelength is much larger than the radius), i.e., the bubble is driven only radially and the primary Bjerknes force is absent. In the absence of translation, the encapsulated bubble is more stable than the gas bubble at all frequencies sampled, i.e., the amplitude threshold, ε_{thr} , is higher for the EMB. The local minima of the lines with solid black circle (for EMB) and red square (for gas bubble) are attributed to the parametric instability, which occurs when $\omega_d \approx \omega_0$ or $2\omega_b/\omega_d$ $\approx n$, where n is a natural number. This shape instability (without translation) arises due to the structure of Mathieu's equation embedded in our model, which was discussed in Refs. 24 and 46. When translation is allowed, the amplitude threshold tends to decrease across all frequencies considered, i.e., the EMBs/bubbles become less stable when they are undergoing translation. We discuss the effects of translation on the shape stability of a gas bubble and an EMB separately.

A. Effects of translation on gas bubble

Figure 2 shows that the decrease in amplitude threshold due to translation is much less appreciable for the gas bubble compared to the EMB. By setting the membrane parameters G_s , G_b , and μ_s to be zero and the surface tension to $\gamma = 0.0729 \,\mathrm{N m^{-1}}$, the mathematical model in Sec. II is suitable for the gas bubble. Therefore, F_{mk} in Eq. (32) is zero. If we temporarily neglect the effects of coupling between the adjacent shape modes, Eq. (31) can be rewritten as

$$M\ddot{a}_k + D\dot{a}_k + Wa_k + G_{k-1} = T,$$
 (37)

where $G_{k-1} = (3/4)v_r^2$ for k = 2 and $G_{k-1} = 0$ for $k \ge 3$. Other coefficients M, D, W, and T are the same as shown in Eq. (32). Similarly, the right-hand side of Eq. (34) is zero, providing the shear-free condition

$$2\mu_{l} \left[\frac{k+2\dot{a}_{k}}{k+1} \frac{\dot{a}_{k}}{R} - \frac{k-1}{k+1} \frac{\dot{R}a_{k}}{R^{2}} - R^{k-2} \int_{R}^{\infty} s^{-k} T_{k}(s,t) ds - \frac{T_{k}(R,t)}{2R} \right] = 0.$$
 (38)

The no-slip condition [Eqs. (35) and (36)] is not applied for the gas bubble. Except for the translational velocity terms, Eqs. (37) and (38) are the same as the equations obtained by Prosperetti³⁹ for a stationary gas bubble. The effect of translation is in W, the coefficient of a_k , for all shape modes, and in G_{k-1} for the second-order shape mode. The relative velocity, v_r , for the cases with $\omega_d/2\pi = 0.1$ and 1 MHz are shown as representative examples in Fig. 3. From Fig. 3, it is clear that the magnitude of v_r is of the order $O(10^{-1})$ m/s. For these cases, the ratio of the effect of translation to surface tension is very small. This can be illustrated by comparing the terms related to these effects that are included in W. Because W is the coefficient of a_k , these terms are likely to be closely related to the natural frequency and, thus, parametric instability. The ratio of these two terms is determined to satisfy the inequality

$$\left(\frac{9(2k^4+3k^3+k^2+k-1)v_r^2}{2(2k-1)(2k+1)(2k+3)R}\right) / \left(\frac{(k+2)(k-1)\gamma}{\rho R^2}\right) < 0.01.$$
(39)

Therefore, the effect of translation on the natural frequency of shape modes is much smaller than the effect of surface tension. Hence, translation plays little effect on the surface stability of a gas bubble for the parameters investigated here. Nevertheless, we find that the amplitude of the shape modes can increase under translation, as shown in Fig. 4 for $\omega_d/2\pi=0.1$ and 1 MHz with the acoustic amplitude slightly smaller than the amplitude threshold. The translation enhances the shape mode amplitudes on the interface of a gas bubble; however, the amplitudes remain small (relative to the initial radius) and, thus, the effect on overall shape stability is not obvious in Fig. 2.

B. Effects of translation on EMB

When the EMB translates due to the primary Bjerknes force imposed by a traveling acoustic plane wave, the amplitude thresholds decrease, as shown in Fig. 2 (the line with blue circles). Consider the case of $\omega_d/2\pi=0.5\,\mathrm{MHz}$ with acoustic intensity $\varepsilon=0.5$. The EMB without translation is stable, as shown in Fig. 5(a), and the initial disturbances to the shape modes damp out with time. By comparison, the second-order shape mode is unstable when the EMB translates due to the acoustic wave [Fig. 5(b)]. The related velocities, including the absolute, relative, and acoustic velocities, are shown in Fig. 5(c).

The interface of an EMB is no-slip, which is different from the free-slip interface of a gas bubble. Therefore, the displacements of material points on the EMB surface in the tangential direction must be considered. The amplitude of tangential displacement is denoted as b_k in Eq. (9). If we neglect the coupling with adjacent modes, neglect the integral $\int_R^\infty [(R/s)^3 - 1](R/s)^k T_k(s,t) ds$, which is much smaller than other integral in Eq. (32) due to the thin boundary layer assumption,²⁴ and eliminate the other integral $\int_R^\infty s^{-k} T_k(s,t) ds$ in Eq. (32) by substituting the no-slip condition [Eq. (36)], then Eq. (31) can be rewritten as

$$\ddot{a}_{k} + \dot{a}_{k} \left[\frac{3\dot{R}}{R} + \frac{4(k+1)\mu_{l}}{\rho R^{2}} + \frac{4(k+1)\mu_{s}}{\rho R^{3}} \right] + \dot{b}_{k} \left[-2k(k+1)^{2} \frac{\mu_{l}}{\rho R^{2}} - 2k(k+1)^{2} \frac{\mu_{s}}{\rho R^{3}} \right] + a_{k} \left[-(k-1)\frac{\ddot{R}}{R} + \frac{4(k+1)\mu_{l}\dot{R}}{\rho R^{3}} \right]$$

$$- \frac{8(k+1)\mu_{s}}{\rho R^{4}} \dot{R} + \frac{2(k+1)G_{s}}{\rho R^{9}} \left(7R_{0}^{6} - R^{6} \right) + \frac{G_{b}}{\rho R^{5}} k(k+1)^{2} (k^{2} + k - 1 + v) - \frac{9(k+1)(2k^{4} + 3k^{3} + k^{2} + k - 1)}{2(2k-1)(2k+1)(2k+3)} \frac{v_{r}^{2}}{R^{2}} \right]$$

$$+ b_{k} \left[-6k(k+1)^{2} \frac{G_{s}R_{0}^{6}}{\rho R^{9}} - k(k+1)^{2} (k^{2} + k - 1 + v) \frac{G_{b}}{\rho R^{5}} + 2k(k+1)^{2} \frac{\mu_{l}\dot{R}}{\rho R^{3}} + 2k(k+1)^{2} \frac{\mu_{s}\dot{R}}{\rho R^{4}} \right] = -k(k+1) \frac{\mu_{l}T_{k}(R,t)}{\rho R^{2}}.$$

$$(40)$$

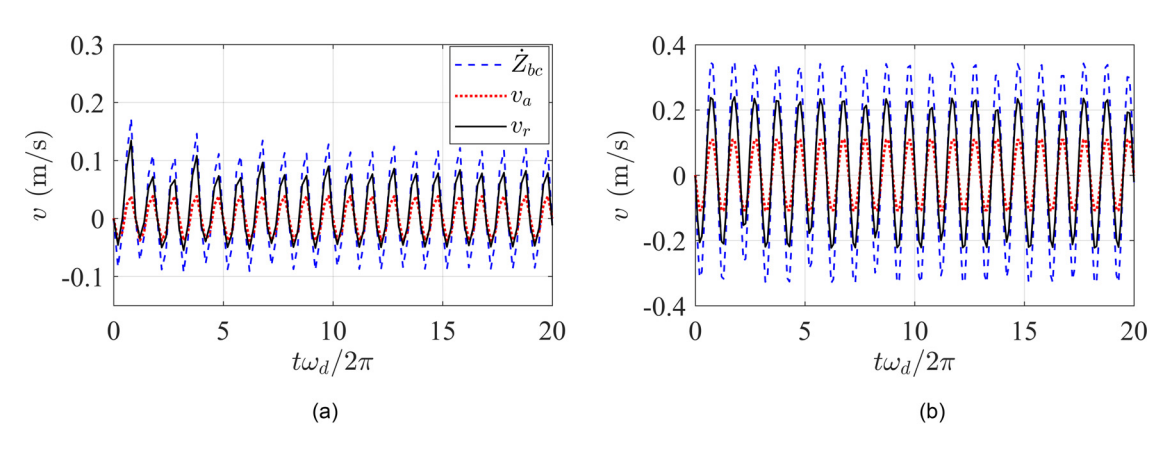


FIG. 3. (Color online) Time evolution of the velocity of bubble translation, \dot{Z}_{bc} , flow velocity due to the acoustic wave, v_a , and relative velocity, $v_r = \dot{Z}_{bc} - v_a$, for gas bubbles with (a) $\omega_d/2\pi = 0.1$ MHz; (b) $\omega_d/2\pi = 1$ MHz. The remaining parameters are the same as in Table I.

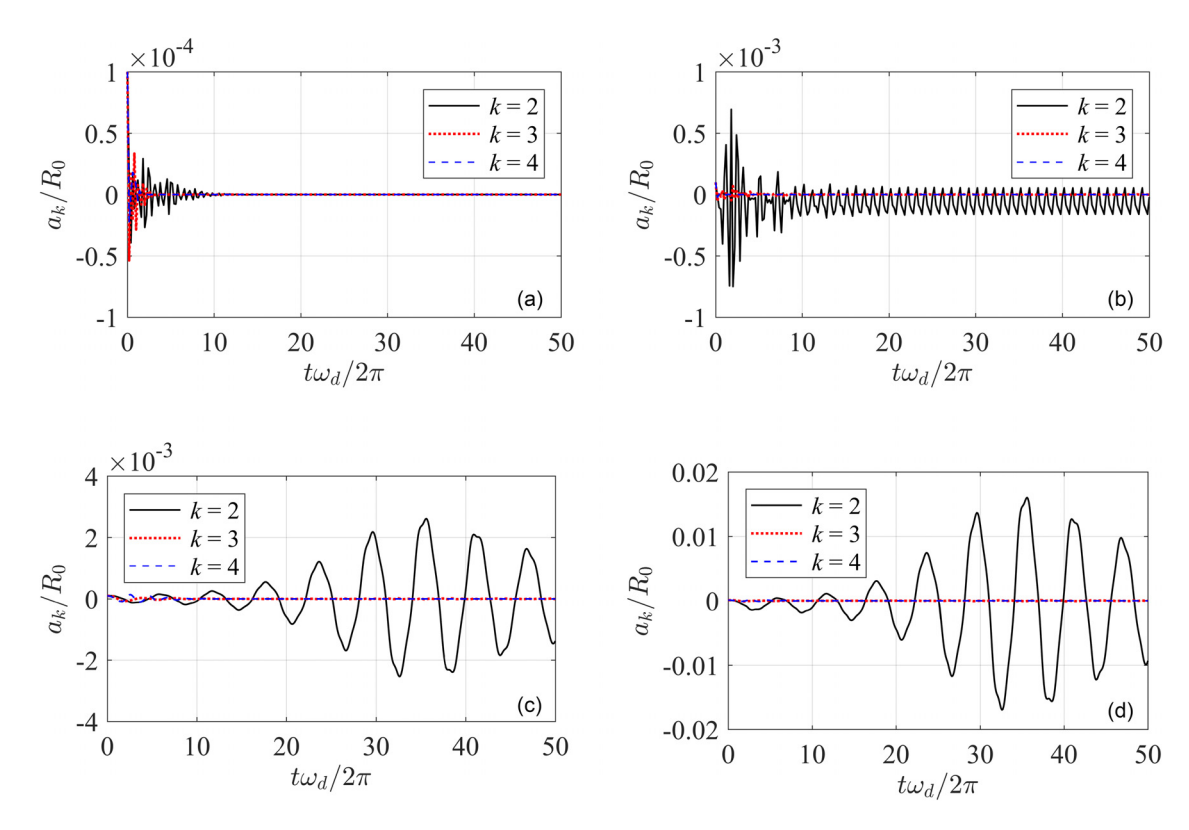


FIG. 4. (Color online) Time evolution of the shape modes for gas bubbles: (a) $\omega_d/2\pi = 0.1$ MHz, $\varepsilon = 0.6$ without translation; (b) $\omega_d/2\pi = 0.1$ MHz, $\varepsilon = 0.6$ with translation; (c) $\omega_d/2\pi = 1$ MHz, $\varepsilon = 1.7$ without translation; (d) $\omega_d/2\pi = 1$ MHz, $\varepsilon = 1.7$ with translation. The remaining parameters are the same as in Table I.

Equation (40) is written in the form of a second-order oscillator equation for a_k . If we neglect the temporal change in the radius, i.e., by letting $\dot{R} = 0$, the coefficients of \dot{a}_k and \dot{b}_k in Eq. (40) are strictly positive and negative, respectively.

The negative coefficient associated with \dot{b}_k implies this term plays a role of *negative* damping, which is destabilizing. The coefficient of b_k is also negative due to the terms associated with G_s and G_b . This suggests that the tangential

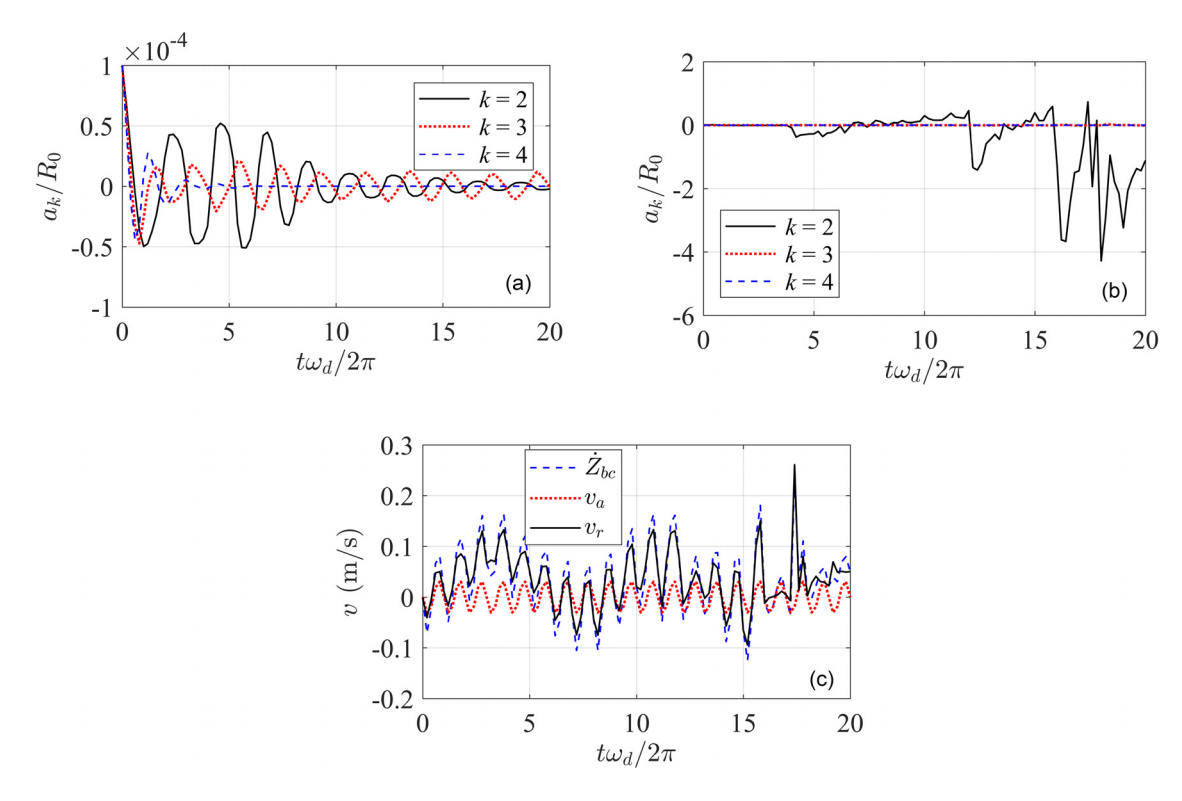


FIG. 5. (Color online) Time evolution of the shape modes for an EMB with $\omega_d/2\pi = 0.5$ MHz, $\varepsilon = 0.5$ without (a) and with (b) translation, and (c) the translational velocities related to (b). The remaining parameters are the same as in Table I.

displacements of the shell act as a destabilizing (or negative) elastic force on the radial shape mode oscillations, a_k .

To demonstrate the destabilizing effect of shear stress on the EMB, we remove the no-slip condition [Eqs. (35) and (36)] and neglect tangential displacements of the shell by setting $b_k = 0$, but still allow translation. While this is not physical, it illustrates that the amplitude thresholds for the surface instability increase under translation when the no-slip condition is neglected, as shown by the green line in Fig. 2. This effect demonstrates that the tangential movement of the material points on the shell (as denoted by b_k) destabilize the interface of the EMB when it translates.

Next, we investigate the stress distribution for the encapsulated bubble. The shapes of the EMB at a_2 / $R_0 = \pm 0.2$ and the relevant stress distributions are shown in Fig. 6. The EMB presents an oblate shape (the thick line in Fig. 6) for $a_2/R_0 = -0.2$ relative to the translational direction, which is also the symmetry axis, and a prolate shape for $a_2/R_0 = 0.2$. The thin lines in Fig. 6 sketch the normal and tangential stresses. For normal stress (left column in Fig. 6), the inward and outward lines show the direction of stress. For tangential stress (right column in Fig. 6), the inward lines represent compression and the outward lines represent tension. For an EMB, the interfacial stress can be compression as well as tension. While the latter tends to reduce the amplitude of the shape modes, the former can cause buckling, which indicates that the membrane stress does not always stabilize the interface. This nature of interfacial stress in an EMB differs from that of a gas bubble, for which the interfacial stress is always tension, i.e., surface tension, which tends to recover the shape of a bubble to that of a

In Eq. (40), which is an oscillator equation, we can regard the term $-k(k+1)(\mu_l/\rho)[T_k(R,t)/R^2]$ as a driving term. Due to the negative sign in front of this term, if the

values of $T_k(R,t)$ and \dot{a}_k are both positive (or negative), it means the driving caused by viscosity $(-k(k+1)(\mu_1/\rho))$ $[T_k(R,t)/R^2]$) is in an opposite direction to the shape mode velocity (\dot{a}_k) , which indicates that viscosity plays a role of damping. In Fig. 7, we plot the time evolution of the velocity of the second-order shape mode, $\dot{a}_2(t)$, and the relevant toroidal field, $T_2(R,t)$. Whether the bubble translates due to the traveling plane wave, or at a constant, prescribed translational velocity (without radial oscillation and applied acoustic pressure), the variations of $\dot{a}_2(t)$ and $T_2(R,t)$ are always in-phase (i.e., of the same sign) for the gas bubble. In contrast, the oscillations of $\dot{a}_2(t)$ and $T_2(R,t)$ are out-of-phase for the EMB. This implies that viscosity may destabilize the interface of an EMB while stabilizing a gas bubble. This difference in behavior for the EMB results from the no-slip boundary condition at the interface. In this case, vorticity generated at the EMB surface requires a finite amount of time to diffuse into the exterior liquid, resulting in a phase lag between the oscillation of the shape mode velocity and the toroidal field.

Next, we consider the effect of higher liquid viscosity, which provides some insight into how translation might affect the shape stability of EMBs in blood. While blood is non-Newtonian and its viscosity varies with the rate of shear, at body temperature, the viscosity of blood is normally about 3–4 times that of water. We therefore investigate the stability of an EMB in a liquid with $\mu_l = 3 \times 10^{-3} \,\mathrm{kg} \;\mathrm{(m \; s)}^{-1}$ and $5 \times 10^{-3} \,\mathrm{kg} \;\mathrm{(m \; s)}^{-1}$, as shown in Fig. 8. The density of blood ($\sim 1060 \,\mathrm{kg/m}^3$) is very near to that of water, therefore, we keep all remaining properties the same as in Table I. The data for liquid viscosity $\mu_l = 1 \times 10^{-3} \,\mathrm{kg} \;\mathrm{(m \; s)}^{-1}$ are reproduced from Fig. 2. In the absence of translation, the results show that the threshold of pressure amplitude, $\varepsilon_{\rm thr}$, for inducing shape instability increases directly with the viscosity of the liquid. Therefore, viscosity plays a significant role in

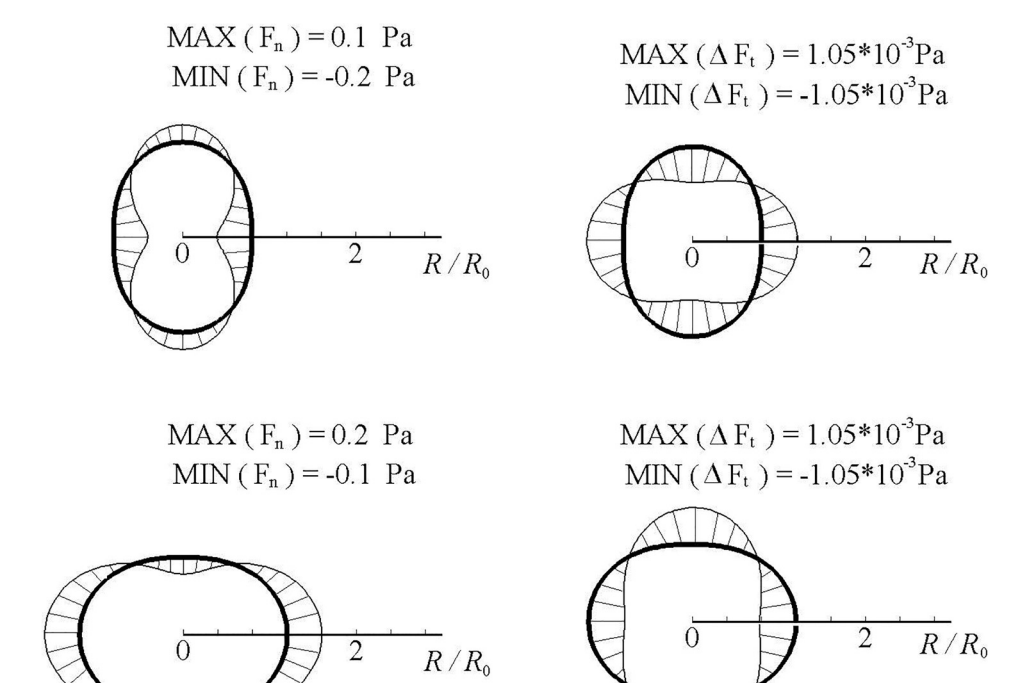


FIG. 6. Shape and stress of an EMB at $a_2/R_0 = \pm 0.2$. The thick lines represent the bubble shape and thin lines show the distribution of stress. The axis of symmetry is shown by the horizontal line through the center of the bubble, which is also the direction of translation. For normal stress (left column), the inward and outward lines show the direction of stress away from the bubble interface. For tangential stress (right column), the inward lines represent compression and the outward lines represent tension. The remaining parameters are the same as in Table I.

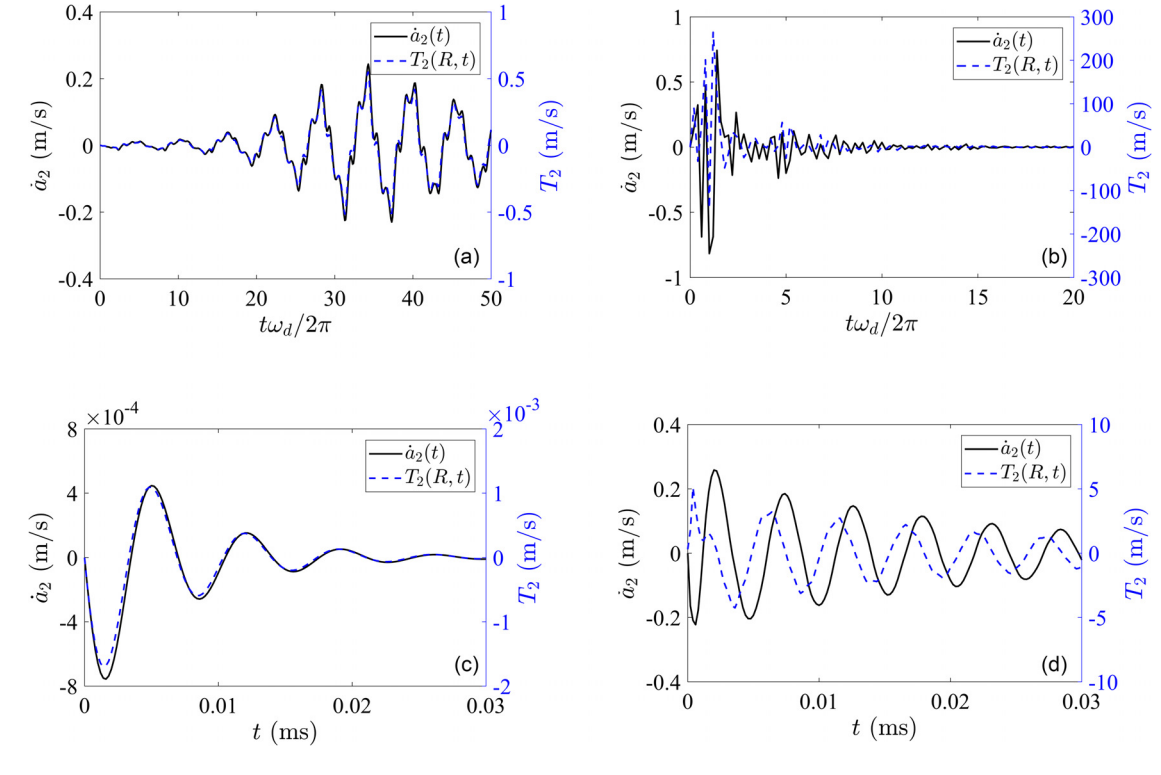


FIG. 7. (Color online) Time evolution of $\dot{a}_2(t)$ and $T_2(R,t)$ for (a) a gas bubble translating under an acoustic wave with $\omega_d/2\pi=1$ MHz and $\varepsilon=1.7$; (b) an EMB translating under an acoustic wave with $\omega_d/2\pi=1$ MHz and $\varepsilon=0.7$; (c) a gas bubble with a constant translational velocity, $v_r=0.01$ m s⁻¹; (d) an EMB with a constant translational velocity, $v_r=0.01$ m s⁻¹. The remaining parameters are the same as in Table I.

stabilizing the EMB shape modes if the translational motion is absent. However, if the EMB translates due to the applied acoustic forcing, the shape stability reduces significantly, and the pressure amplitude threshold is nearly the same for the three different liquid viscosities. These results suggest that, while a higher liquid viscosity can inhibit shape instability when the bubble is stationary, it has minimal effect on shape stability during translation. Furthermore, translation

causes a greater *reduction* in shape stability as the liquid viscosity is increased. This supports the above analysis that the destabilizing effect of translation on an EMB is mediated by the interfacial viscous stress resulting from the no-slip boundary condition.

We further investigate the EMB with various elastic moduli: $G_s = 0.3$, 0.5, and 0.7 N m⁻¹. Similar stability phenomena are revealed in Fig. 9, which shows that the

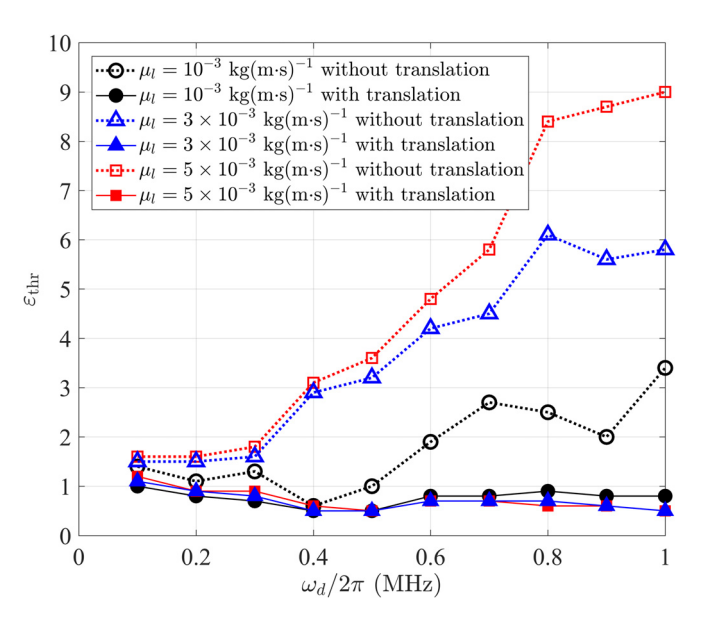


FIG. 8. (Color online) Threshold of acoustic pressure amplitude, $\varepsilon_{\rm thr}$, for inducing shape instability of an EMB versus driving frequency, ω_d , with $\mu_l=1\times 10^{-3}\,{\rm kg~(m\cdot s)^{-1}}$, $3\times 10^{-3}\,{\rm kg~(m~s)^{-1}}$ and $5\times 10^{-3}\,{\rm kg~(m~s)^{-1}}$, with and without translation. The remaining parameters are the same as in Table I.

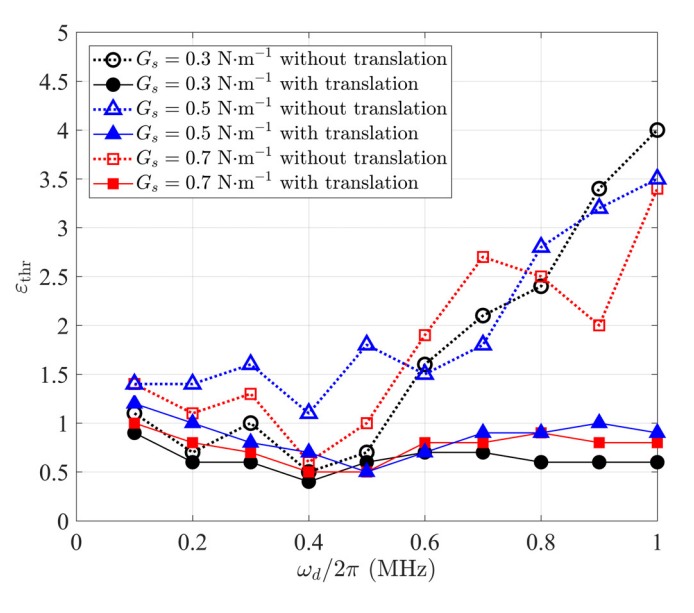


FIG. 9. (Color online) Threshold of acoustic pressure amplitude, $\varepsilon_{\rm thr}$, for inducing shape instability of an EMB versus driving frequency, ω_d , with $G_s = 0.3 \, {\rm N \ m^{-1}}$, $G_s = 0.5 \, {\rm N \ m^{-1}}$, and $G_s = 0.7 \, {\rm N \ m^{-1}}$, with and without translation. The remaining parameters are the same as in Table I.

instability threshold for the EMBs undergoing translation is smaller than when translation is absent. Especially for higher driving frequencies, the EMBs without translation are highly stable, i.e., the thresholds are much larger than those with translation.

IV. CONCLUSIONS

A theoretical study is carried out for the nonspherical shape modes of EMBs and gas bubbles translating subject to a traveling acoustic plane wave. An approximate model is developed that considers the interactions among the external liquid flow, nonspherical deformation of the membrane, and the expansion/compression of the internal gas. The potential flow in the bulk volume of the external flow is modeled using an asymptotic analysis. Viscous effects within the thin boundary layer at the liquid-membrane interface are included using Prosperetti's theory. In-plane stress and the bending moment of EMBs are incorporated into the dynamic boundary condition at the interface. The evolution equations for the volume mode, translation, and shape modes of an EMB are thus derived.

The results show that translation only slightly destabilizes the interface of an uncoated gas bubble. This phenomenon is not obvious as the destabilizing effect of translation is much smaller than the stabilizing effect of surface tension in the cases considered. By comparison, translation has a much greater destabilizing effect on an EMB. This effect is attributed to the interfacial viscous stress owing to the no-slip condition at the EMB-liquid interface, as compared to the zero stress condition that results from the free-slip condition at the gas-bubble interface. In particular, the no-slip boundary condition incites shape instability of the EMB through the tangential motion of the material points at the interface and the compression stress in the shell. Furthermore, while higher liquid viscosity enhances shape stability when an EMB is stationary, it appears to have little effect on stability under translation.

ACKNOWLEDGMENTS

This work was partially supported by the National Natural Science Foundation of China (Grant No. 11772196) and Engineering and Physical Sciences Research Council (UK) (EPSRC) Grant No. EP/P015743/1.

APPENDIX: DERIVATION OF THE COEFFICIENTS q_k IN EQS. (15)–(17)

The coefficients q_k are determined by the kinematic boundary condition Eq. (13), which is rewritten as

$$\frac{\partial S}{\partial t} + \left(\nabla \varphi - \dot{Z}_{bc} \mathbf{e}_z\right) \cdot \nabla S = 0, \tag{13}$$

where the surface function S is defined in Eq. (14). The first term of Eq. (13) is written explicitly as

$$\frac{\partial S}{\partial t} = -\dot{R} - \sum_{k=2}^{\infty} \dot{a}_k P_k(\cos \theta). \tag{A1}$$

The second term of Eq. (13) is written as

$$\nabla \varphi \cdot \nabla S = \frac{\partial \varphi}{\partial r} \frac{\partial S}{\partial r} + \frac{1}{r} \frac{\partial \varphi}{\partial \theta} \frac{1}{r} \frac{\partial S}{\partial \theta} = \frac{\partial \varphi}{\partial r} - \frac{1}{r} \frac{\partial \varphi}{\partial \theta} \sum_{k=2}^{\infty} \frac{a_k}{r} P_k^1(\cos \theta). \tag{A2}$$

Substituting the form of velocity potential [Eq. (12)], Eq. (A2) becomes

$$\nabla \varphi \cdot \nabla S = -\frac{q_0}{r^2} + \left(v_a - 2\frac{q_1}{r^3}\right) P_1 - \sum_{k=2}^{\infty} (k+1)$$

$$\times \frac{q_k}{r^{k+2}} P_k - \sum_{k=2}^{\infty} \left(v_a + \frac{q_1}{r^3}\right) \frac{a_k}{r} P_1^1 P_k^1. \tag{A3}$$

If we expand Eq. (A3) in a Taylor series about $r = R + \sum_{k=2}^{\infty} a_k P_k(\cos \theta)$ with $a_k/R \ll 1$, then we get

$$\nabla \varphi \cdot \nabla S = -\frac{q_0}{R^2} + \left(v_a - 2\frac{q_1}{R^3}\right) P_1 + \frac{6q_1}{R^4} \sum_{k=2}^{\infty} a_k P_1 P_k$$

$$+ \sum_{k=2}^{\infty} \left(\frac{2q_0}{R^3} a_k - (k+1)\frac{q_k}{R^{k+2}}\right) P_k$$

$$- \sum_{k=2}^{\infty} \left(v_a + \frac{q_1}{R^3}\right) \frac{a_k}{R} P_1^1 P_k^1. \tag{A4}$$

Next, we introduce the following relations of the Legendre polynomials,

$$\sum_{k=2}^{\infty} a_k P_1 P_k = \sum_{k=2}^{\infty} \left(\frac{k+1}{2k+3} a_{k+1} + \frac{k}{2k-1} a_{k-1} \right) P_k, \quad (A5)$$

and

$$\sum_{k=2}^{\infty} a_k P_1^1 P_k^1 = \sum_{k=2}^{\infty} \left(\frac{(k+1)(k+2)}{2k+3} a_{k+1} - \frac{k(k-1)}{2k-1} a_{k-1} \right) P_k.$$
(A6)

After applying Eqs. (A5) and (A6), Eq. (A4) reduces to

$$\nabla \varphi \cdot \nabla S = -\frac{q_0}{R^2} + \left[v_a - 2\frac{q_1}{R^3} + \frac{12q_1}{5R^4} a_2 - \frac{6}{5} \left(v_a + \frac{q_1}{R^3} \right) \frac{a_2}{R} \right] P_1 + \sum_{k=2}^{\infty} \left[\frac{2q_0}{R^3} a_k - (k+1) \right] \times \frac{q_k}{R^{k+2}} + \frac{6q_1}{R^4} \left(\frac{k+1}{2k+3} a_{k+1} + \frac{k}{2k-1} a_{k-1} \right) - \left(\frac{v_a}{R} + \frac{q_1}{R^4} \right) \left(\frac{(k+1)(k+2)}{2k+3} a_{k+1} - \frac{k(k-1)}{2k-1} a_{k-1} \right) \right] P_k.$$
(A7)

Similary, we derive the third term of Eq. (13) as

$$\dot{Z}_{bc}\mathbf{e}_{z} \cdot \nabla S = \dot{Z}_{bc}P_{1} - \sum_{k=2}^{\infty} \frac{a_{k}}{r} \dot{Z}_{bc}P_{1}^{1}P_{k}^{1}$$

$$= \left(\dot{Z}_{bc} - \frac{6a_{2}}{5R} \dot{Z}_{bc}\right) P_{1} - \sum_{k=2}^{\infty} \dot{Z}_{bc}$$

$$\times \left(\frac{(k+1)(k+2)a_{k+1}}{2k+3R} - \frac{k(k-1)a_{k-1}}{2k-1R}\right) P_{k}.$$
(A8)

Substituting Eqs. (A1), (A7), and (A8) into Eq. (13) and utilizing the orthogonality of the Legendre polynomials, we obtain the expressions for q_k shown in Eqs. (15)–(17).

- ¹K. Ferrara, R. Pollard, and M. Borden, "Ultrasound microbubble contrast agents: Fundamentals and application to gene and drug delivery," Ann. Rev Biomed. Eng. **9**, 415–447 (2007).
- ²C. C. Coussios and R. A. Roy, "Applications of acoustics and cavitation to noninvasive therapy and drug delivery," Annu. Rev. Fluid Mech. 40, 395–420 (2008).
- ³A. Delalande, M. Postema, N. Mignet, P. Midoux, and C. Pichon, "Ultrasound and microbubble-assisted gene delivery: Recent advances and ongoing challenges," Ther. Delivery 3, 1199–1215 (2012).
- ⁴F. Calliada, R. Campani, O. Bottinelli, A. Bozzinni, and M. G. Sammaruga, "Ultrasound contrast agents: Basic principles," Eur. J. Radiol. 27, S157–S190 (1998).
- ⁵B. Dollet, S. M. van der Meer, V. Garbin, N. de Jong, D. Lohse, and M. Versluis, "Nonspherical oscillations of ultrasound contrast agent micro-ubbles," Ultrasound Med. Biol. **34**, 1465–1473 (2008).
- ⁶V. F. K. Bjerknes, *Fields of Force* (Columbia University Press, New York, 1906).
- ⁷P. A. Dayton, K. E. Morgan, A. L. Klibanov, G. Brandenburger, K. R. Nightingale, and K. W. Ferrara, "A preliminary evaluation of the effects of primary and secondary radiation forces on acoustic contrast agents," IEEE Trans. Ultrason. Ferroelectr. Freq. Control 44, 1264–1277 (1997).
- ⁸C. D. Ohl, M. Arora, R. Ikink, N. de Jong, M. Veersluis, M. Delius, and D. Lohse, "Sonoporation from jetting cavitation bubbles," Biophys. J. 91, 4285–4295 (2006).
- ⁹A. van Wamel, K. Kooiman, M. Harteveld, M. Emmer, F. J. ten Cate, M. Versluis, and N. de Jong, "Vibrating microbubbles poking individual cells: Drug transfer into cells via sonoporation," J. Control. Release 112, 149–155 (2006).
- ¹⁰T. B. Benjamin and A. T. Ellis, "Self-propulsion of asymmetrically vibrating bubbles," J. Fluid Mech. 212, 65–80 (1990).
- ¹¹H. Takahira, T. Akamatsu, and S. Fujikawa, "Dynamics of two nonspherical bubbles in a viscous liquid," Trans. JSME B 57, 447–455 (1991).
- ¹²A. A. Doinikov, "Translational motion of a bubble undergoing shape oscillations," J. Fluid Mech. 501, 1–24 (2004).
- ¹³Z. C. Feng and L. G. Leal, "Nonlinear bubble dynamics," Annu. Rev. Fluid Mech. 29, 201–243 (1997).
- ¹⁴A. J. Reddy and A. J. Szeri, "Coupled dynamics of translation and collapse of acoustically driven microbubbles," J. Acoust. Soc. Am. 112, 1346–1352 (2002).
- ¹⁵A. J. Reddy and A. J. Szeri, "Shape stability of unsteadily translating bubbles," Phys. Fluids 14, 2216–2224 (2002).
- ¹⁶M. L. Calvisi, O. Lindau, J. R. Blake, and A. J. Szeri, "Shape stability and violent collapse of microbubbles in acoustic traveling waves," Phys. Fluids 19, 047101 (2007).
- ¹⁷S. J. Shaw, "Translation and oscillation of a bubble under axisymmetric deformation," Phys. Fluids 18, 072104 (2006).
- ¹⁸S. Shaw, "The stability of a bubble in a weakly viscous liquid subject to an acoustic traveling wave," Phys. Fluids 21, 022104 (2009).
- ¹⁹J. E. Chomas, P. A. Dayton, D. May, J. Allen, A. Klibanov, and K. Ferrara, "Optical observation of contrast agent destruction," Appl. Phys. Lett. 77, 1056–1058 (2000).
- ²⁰M. Postema, A. van Wamel, C. T. Lancee, and N. de Jong, "Ultrasound-induced encapsulated microbubble phenomena," Ultrasound Med. Biol. 30, 827–840 (2004).

- ²¹K. Tsiglifis and N. A. Pelekasis, "Parametric stability and dynamic buckling of an encapsulated microbubble subject to acoustic disturbances," Phys. Fluids 23, 012102 (2011).
- ²²K. Tsiglifis and N. A. Pelekasis, "Simulations of insonated contrast agents: Saturation and transient break-up," Phys. Fluids 25, 032109 (2013).
- ²³Y. Liu, K. Sugiyama, S. Takagi, and Y. Matsumoto, "Numerical study on the shape oscillation of an encapsulated microbubble in ultrasound field," Phys. Fluids 23, 041904 (2011).
- ²⁴Y. Liu, K. Sugiyama, S. Takagi, and Y. Matsumoto, "Surface instability of an encapsulated bubble induced by an ultrasonic pressure wave," J. Fluid Mech. 691, 315–340 (2012).
- ²⁵Q. X. Wang, K. Manmi, and M. L. Calvisi, "Numerical modeling of the 3D dynamics of ultrasound contrast agent microbubbles using the boundary integral method," Phys. Fluids 27, 022104 (2015).
- ²⁶Y. Liu, M. L. Calvisi, and Q. X. Wang, "Nonlinear oscillation and interfacial stability of an encapsulated microbubble under dual-frequency ultrasound," Fluid Dyn. Res. 49, 025518 (2017).
- ²⁷P. A. Dayton, J. S. Allen, and K. W. Ferrara, "The magnitude of radiation force on ultrasound contrast agents," J. Acoust Soc. Am. 112, 2183–2192 (2002).
- ²⁸A. Delalande, S. Kotopoulis, M. Postema, P. Midoux, and C. Pichon, "Sonoporation: Mechanistic insights and ongoing challenges for gene transfer," Gene 525, 191–199 (2013).
- ²⁹H. Chen, A. A. Brayman, W. Kreider, M. R. Bailey, and T. J. Matula, "Observations of translation and jetting of ultrasound-activated microbubles in mesenteric microvesels," Ultrasound Med. Biol. 37, 2139–2148 (2011).
- ³⁰M. Strasberg and T. B. Benjamin, "Excitation of oscillations in the shape of pulsating bubbles—Experimental work," J. Acoust. Soc. Am. 30, 697 (1958).
- ³¹L. A. Crum and A. I. Eller, "Motion of bubbles in a stationary sound field," J. Acoust. Soc. Am. 48, 181–189 (1970).
- ³²Z. C. Feng and L. G. Leal, "On energy transfer in resonant bubble oscillations," Phys. Fluids A 5, 826–836 (1993).
- ³³Z. C. Feng and L. G. Leal, "Translational instability of a bubble undergoing shape oscillations," Phys. Fluids 7, 1325–1336 (1995).
- ³⁴P. G. Saffman, "The self-propulsion of a deformable body in a perfect fluid," J. Fluid Mech. 28, 385–389 (1967).
- ³⁵C. C. Mei and X. Zhou, "Parametric resonance of a spherical bubble," J. Fluid Mech. 229, 29–50 (1991).
- ³⁶Y. A. Itkulova, O. A. Abramova, N. A. Gumerov, and I. S. Akhatov, "Boundary element simulations of free and forced bubble oscillations in potential flow," Proc. ASME Inter. Mech. Eng. Cong. Expo. 7, 36972 (2014)
- ³⁷X. Xi, F. Cegla, R. Mettin, F. Holsteyns, and A. Lippert, "Study of non-spherical bubble oscillations near a surface in a weak acoustic standing wave field," J. Acoust. Soc. Am. 135, 1731–1741 (2014).
- ³⁸A. A. Doinikov and P. A. Dayton, "Spatio-temporal dynamics of an encapsulated gas bubble in an ultrasound field," J. Acoust. Soc. Am. 120, 661–669 (2006).
- ³⁹A. Prosperetti, "Viscous effects on perturbed spherical flows," Q. Appl. Math. 34, 339–352 (1977).
- ⁴⁰Q. X. Wang and J. R. Blake, "Non-spherical bubble dynamics in a compressible liquid. Part 1. Travelling acoustic wave," J. Fluid Mech. 659, 191–224 (2010).
- ⁴¹A. E. Green and J. E. Adkins, *Large elastic deformations and non-linear continuum mechanics* (Clarendon Press, Oxford, 1960).
- ⁴²M. Mooney, "A theory of large elastic deformation," J. Appl. Phys. 11, 582–592 (1940).
- ⁴³A. E. H. Love, "The small free vibrations and deformation of a thin elastic shell," Philos. Trans. R. Soc. A **179**, 491–546 (1888).
- ⁴⁴Y. Liu, K. Sugiyama, and S. Takagi, "On the interaction of two encapsulated bubbles in an ultrasound field," J. Fluid Mech. 804, 58–89 (2016).
- ⁴⁵L. Hoff, P. C. Sontum, and J. M. Hovem, "Oscillations of polymeric microbubbles: Effect of the encapsulating shell," J. Acoust. Soc. Am. 107, 2272–2280 (2000).
- ⁴⁶Y. Liu and Q. Wang, "Stability and natural frequency of nonspherical mode of an encapsulated microbubble in a viscous liquid," Phys. Fluids 28, 062102 (2016).
- ⁴⁷H. Lamb, *Hydrodynamics* (Cambridge University Press, Cambridge, UK, 1932).